JOURNAL OF APPLIED ELECTROCHEMISTRY **28** (1998) 237–243

Modelling coupled transfers in an industrial fluorine electrolyser*

H. ROUSTAN, J. P. CAIRE

LEPMI, ENSEEG, UMR 5631 INPG–CNRS, 1130 Rue de la Piscine, 38402 Saint Martin d'Hères, France

F. NICOLAS

COMURHEX, BP 29, 26701 Pierrelatte Cedex, France

P. PHAM

SINULOG, Bât 1, 60, Rue Lavoisier, 38330 Rontbonnet Saint Martin, France

Received 19 December 1996; revised 24 February 1997

The construction of efficient electrolysers requires a detailed knowledge of the mass flows, currents and temperatures in the cell. The paper describes three successive models designed for modelling transfers in an industrial electrolysis cell for fluorine production. The conservation laws for charge, mass and energy are approximated by use of a Galerkin finite element code. The solution of coupled transfers is necessary to describe the thermal behaviour of the cell. The method used here may be extended to the modelling of other electrochemical cells.

Keywords: *coupled transfers*, *fluorine*, *electrolyser*

List of symbols

C_p	Specific heat ($J\,kg^{-1}\,K^{-1}$)
E	reversible cell potential (V)
E_{thn}	thermoneutral potential (V)
F	Faraday constant ($96\,485\,C\,mol^{-1}$)
g	acceleration of gravity ($m\,s^{-2}$)
h	heat transfer coefficient ($W\,m^{-2}\,K^{-1}$)
i	local current density ($A\,m^{-2}$)
I	current (A)
JNF	input current density on the busbar ($A\,m^{-2}$)
k	thermal conductivity ($W\,m^{-1}\,K^{-1}$)
$\boldsymbol{n}$	normal vector
n_e	number of electrons
P	pressure (Pa)
Pe_M	mesh Peclet number
Q_{th}	volumetric rate of thermal losses ($W\,m^{-3}$)
R	electrolyte resistance (Ω)
S	entropy ($J\,mol^{-1}\,K^{-1}$)
T	temperature (K)
T_{amb}	ambient temperature (K)
U	cell measured potential (V)
$\boldsymbol{v}$	fluid velocity vector ($m\,s^{-1}$)
v_x, v_y	cartesian components of the velocity vector ($m\,s^{-1}$)
V	potential (V)
Δl	length of a mesh in the flow direction (m)

Greek symbols

α_i	arbitrary test function
δ	interface thickness (m)
ε	surface emissivity
μ	electrolyte dynamic viscosity ($kg\,m^{-1}\,s^{-1}$)
η_a	anodic overpotential (V)
η_c	cathodic overpotential (V)
ρ	density ($kg\,m^{-3}$)
σ	electric conductivity ($S\,m^{-1}$)
σ_{int}	equivalent electric conductivity ($S\,m^{-1}$)
σ_{SB}	Stephan–Boltzmann constant ($W\,m^{-2}\,K^{-4}$)
∇	gradient
$\nabla\cdot$	divergence

1. Introduction

There is substantial literature on numerical models devoted to current distribution, thermal problems and fluid mechanics in electrochemical cells [1]. Most work is illustrated by simple geometry problems and few papers deal with the potential field, heat and mass distribution, and coupled transfers [2]. Modelling electrochemical cells is an economic challenge [3] which has led to scientific problems in the molten salt field being approached in relation to aluminium [4–7] and fluorine production [8].

2. Specific features of the fluorine cells

Fluorine evolving carbon anodes exhibit unusually high overpotentials generated, according to Conway [9–11], by the effect of a nonohmic charge transfer

* This paper was presented at the Fourth European Symposium on Electrochemical Engineering, Prague, 28–30 August 1996.

barrier layer due to 'CF' film formation. Moreover, due to difficulties of fluorine bubble detachment, a special adherent gas film is formed on the anode. The KF–2HF molten salt electrolyte used in the fluorine industry in corrosive and its physical properties, especially its thermal conductivity, are not well known. This physical property is a key parameter in the modelling of coupled transfers in this type of electrolytic cell and its determination is essential. No data concerning the thermal conductivity of the KF–2HF molten salt used in industrial fluorine electrolysis have been found in the literature. This parameter was obtained experimentally [12].

The electrolyser also has specific characteristics [13]. A fluorine cell requires the presence of skirts placed between anodes and cathodes in order to separate the evolved gases and prevent explosive recombination of F_2 and H_2. Due to these skirts, the anode–cathode distance is large, leading to considerable ohmic drop and large Wagner numbers. The unusual overpotentials encountered create strong irreversibility at each electrode leading to significant thermal losses. Thus, there is a considerable interaction between electrical and thermal modelling and it is necessary to model the cell by considering strong numerical coupling between the electrical and thermal equations.

The strongly coupled transfer appearing are *a priori* too complex to be modelled directly. Three successive models of increasing complexity are therefore presented here on the basis of an electrolyser slightly different from the industrial cell for reasons of confidentiality.

3. Modelling of the electrolytic cell behaviour

Flux-Expert® (F.E.) [14], a commercial software tool designed for the numerical modelling of miscellaneous physical problems was used. This code is based on the Galerkin finite element method [15]. This method, compared to other numerical methods [16–18], is particularly well adapted to solving coupled partial differential equations with peculiar boundary conditions and complex geometry. In contrast to methods using a constant step rectangular mesh, the finite element method allows the use of a very fine mesh in the regions requiring special attention and a larger mesh elsewhere. Moreover, in contrast to most software, F.E. is not written for a particular class of problem only, and a part of the code can easily be modified by an experienced user [19] to define specific F.E. equations describing complex coupled problems. This feature is described in the Appendix. It is used to generate the F.E. equations described in the paper.

The primary current distribution is obtained from the solution of the Laplace equation:

$$\nabla(-\sigma\nabla V) = 0 \tag{1}$$

This equation may be solved with different boundary conditions related to current or potential:

$$V = \text{constant} \tag{2}$$

$$-\sigma(\nabla V \boldsymbol{n}) = 0 \tag{3}$$

$$-\sigma(\nabla V \boldsymbol{n}) = JNF \tag{4}$$

corresponding, respectively, to a Dirichlet condition used for an imposed potential (2), a homogeneous Von Neumann condition applied to insulated walls (3), and a nonhomogeneous Von Neumann condition (4) used to impose a uniform current density, JNF.

The Laplace equation (1) was solved for a 2D cross section of a schematic industrial cell of a $0.480\,\text{m} \times 0.857\,\text{m}$ cross section. For reasons of symmetry and computer efficiency, only half a cell is studied, as shown in Fig. 1. The calculations were made by applying boundary conditions of type (4) on the upper edge of the bus bar (Fig. 1) and $V = 0$ of type (2) on both cathodes.

The solver supplies a fast and accurate potential distribution. The current vectors are postprocessed from the gradients of computed potentials. The equipotential curve map is reasonable (Fig. 2) and the computed current density vectors shows a satisfactory appearance (Figs 3 and 4). Since the skirts and the tank are made of conducting metals, some current flow is seen in both the conducting skirts and the tank. However, comparison of the numerical results obtained from the model to measurements shows that the computed cathode–anode potential drop was far less than that observed. This confirms that modelling the secondary distribution of current is an essential condition for obtaining realistic potentials.

The secondary current distribution is characterized by a steep potential interfacial discontinuity in the fluorine case. For example, a 2.5 V anodic potential drop is observed for a typical mean anodic current density of $2000\,\text{A}\,\text{m}^{-2}$. Modelling such a potential

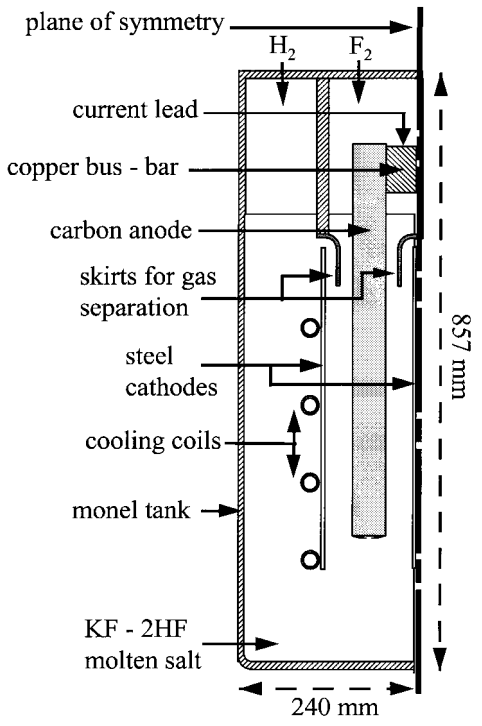

Fig. 1. Schematic crosssection of one half of a fluorine cell.

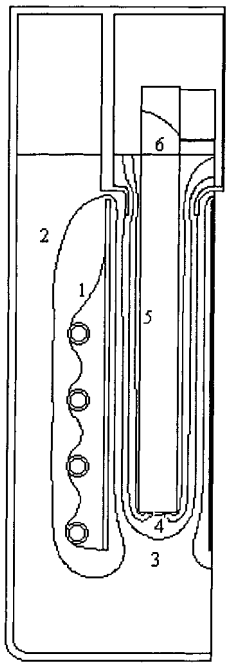

Fig. 2. Equipotential curves for primary current distribution. Key: (1) 0.0 V; (2) 0.4 V; (3) 0.8 V; (5) 1.2 V; (6) 2.0 V.

step is *a priori* incompatible with the finite element method which postulates the continuity of the main variable (e.g., the potential) [15]. The method developed to overcome this difficulty [20] is described elsewhere [21]. The basic idea consists of introducing a hypothetical very thin resistive layer with an unknown electrical conductivity σ_{int} at the interface (Fig. 5(a)). This layer is not meshed but is taken into account by use of a special F.E. linear finite element

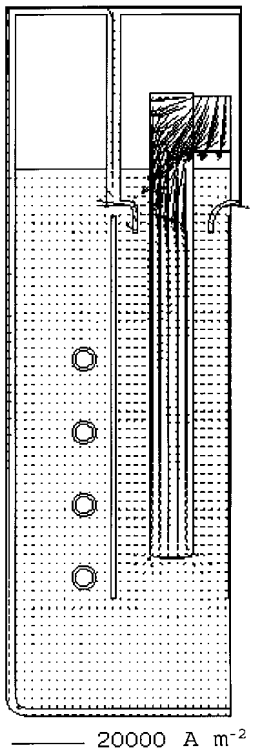

Fig. 3. Secondary current density distribution.

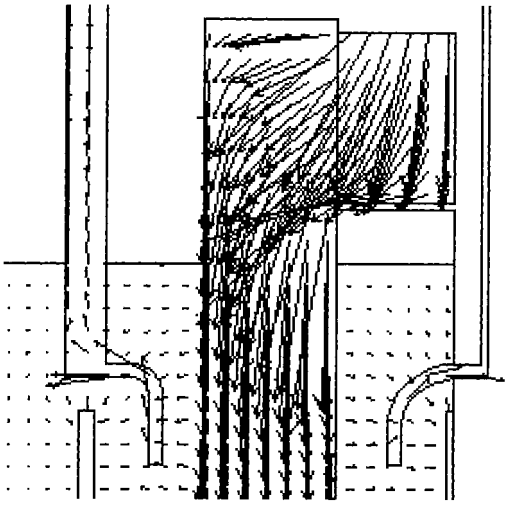

Fig. 4. Close-up current flowing from bus bar to anode.

named termed an interfacial element [21]. The electrical conductivity, σ_{int}, of the pseudo-element depends on both the resistive layer thickness, δ, and the local current density according to a Tafel or Butler–Volmer law or an experimental data file. Using the plan of Fig. 5, the requirement of potential continuity is satisfied in the thin layer, and the secondary distribution can then be solved as a primary distribution. The solution is obtained using an iterative process to compute in sequence; an initial global potential distribution, an equivalent electrical conductivity σ_{int}, an interfacial current density in the layer, a local overpotential, a new global potential etc. In some works the electrode conductivity is assumed to be infinitely large to avoid this computation. One main advantage of this method is that the current density distribution required by the thermal equation is obtained in all the cell elements, including electrodes and busbar.

Potential measurements made with small copper wires placed in a full scale fluorine pilot electrolyser

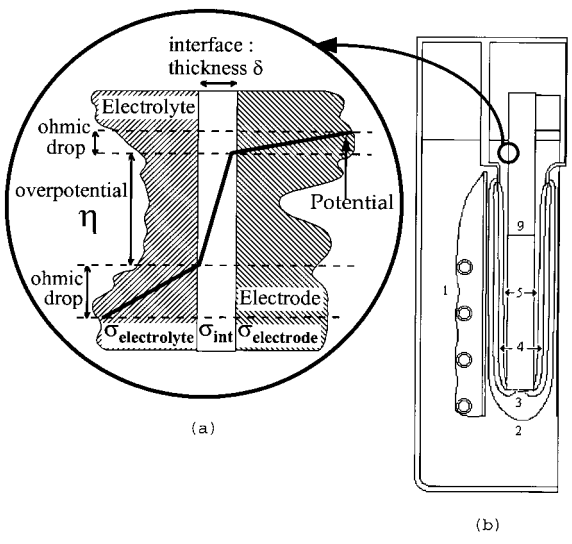

Fig. 5. Schematic illustration of the secondary current distribution model (a) and related equipotential curves (b). Key: (1) 0.0 V; (2) 0.5 V; (3) 1.0 V; (4) 1.5 V; ... (9) 9.5 V.

[22] showed a fairly good, 95% , agreement between experiments and numerical results. Thus, there is no need to solve the tertiary current distribution since the model reflects the real electrokinetic behaviour of the cell (Fig. 5(b)).

4. Modelling of the thermal cell behaviour

The thermal behaviour is a key feature for a fluorine cell since hot spots can induce local corrosion problems on various fragile parts of the cell, while too low a temperature can locally freeze the molten salt. Both phenomena are undesired and can lead to a significant reduction in the life of the electrolyser. Thus a realistic prediction of the isotherms is needed in order to find a set of optimal conditions leading to a convenient uniformity of the temperature field in the cell.

In the first step, a global thermal balance was made to determine all the heat transfer terms involved in the cell [23]. Several thermal flows are easily estimated:

(i) Convection and radiation at external surfaces of the electrolyser may easily be calculated when the wall temperature and the ambient temperature are measured from an estimation of the convection coefficient, h, using the McAdams correlation [24].
(ii) The cooling thermal flows due to the coils are estimated from temperatures and water flow rates measured at the cell inlet and outlet.
(iii) The enthalpy carried by both gases is obtained from temperature and gas flow rate measurements.

In such a high current density process, large quantities of heat are generated through irreversibility phenomena (overpotentials and ohmic drop). The total heat production, Q_{th}, is the sum of the irreversible and reversible sources:

$$Q_{th} = (U - E)i - \frac{i}{n_e F} T\Delta S \tag{5}$$

The last term in Equation 5 is difficult to compute. It is, therefore, easier to use the concept of the thermoneutral potential, E_{thneut}, defined as the potential applied when the heat losses due to irreversibility of reaction exactly compensate the heat of reaction [25]. E_{thneut} was obtained from measurements on a small scale pilot plant electrolyser maintained at thermal equilibrium [22]. The global heat losses, Q_{th}, at each point of the cell depend on both the applied cell potential U and E_{thneut}:

$$Q_{th} = (U - E_{thneut})i \tag{6}$$

Irreversibilities arise from overpotentials and ohmic drop included in the U term and generate two different heat sources. Since overpotentials originate at the electrode interface, the model computes overpotential, local heating at the electrode interface and the ohmic drop in every conducting part of the cell.

Since the physical properties of each cell material also depend on the local temperature, the following set of coupled partial differential equations must be solved:

$$\begin{cases} \nabla(-\sigma\ \nabla V) = 0 \\ \nabla(-k\ \nabla T) = Q_{th} \end{cases} \tag{7}$$

V and T, k and σ play a symmetrical role in these equations. The boundary conditions are similar to Equations (2–4) but the thermal equation implies an additional Fourier condition at the outer walls of the cell:

$$-k(\nabla T \boldsymbol{n}) = h(T - T_{amb}) + \sigma_{SB}\varepsilon\left(T^4 - T_{amb}^4\right) \tag{8}$$

The final equation takes into account convection and radiation effects at the outer walls of the cell. Equations 7 and 8 were solved simultaneously using an original F.E. equation and a Newton–Raphson algorithm.

The resulting maps for equipotential curves and current density vectors are similar to those obtained with the previous model (Fig. 5(b)). The calculated isotherms seem realistic (Fig. 6), for it appears that the centre of the cell is warmer than the peripheral zones, which are cooled by coils, wall advection and radiation.

These calculations were made using an estimated thermal conductivity of the KF–2HF molten salt [12]. However, the range of temperatures obtained from the model does not correspond to measurements. In this model, the thermal conductivity had to be artificially increased to 20 $W\,m^{-1}\,K^{-1}$ to correspond to the thermal observations (Fig. 7). Such an overesti-

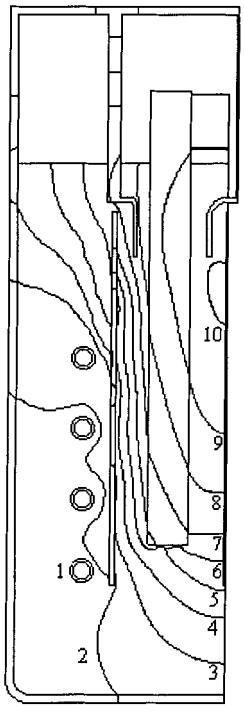

Fig. 6. Temperature profiles computed with the actual value of k. Temperatures: (1) 325 K; (2) 340 K; (3) 355 K; (4) 370 K; (5) 385 K; (6) 400 K; (7) 415 K; (8) 430 K; (9) 445 K; (10) 457 K.

mated conduction may be interpreted as a compensation for the internal advection which was neglected in this calculation. In fact these results suggest that a gravity gradient, due to temperature profiles and bubble effects, induces some inner convection which homogenizes the temperature profiles in the cell. This effect requires modification of the model by the coupling of Equations 7 with the Navier–Stokes equations.

5. Hydrodynamic model of the cell

The model is based on the assumption that the bubble effects can be neglected, so the model includes the previous equations and the Navier–Stokes equations for noncompressible single phase Newtonian fluids:

$$\nabla(-\sigma\nabla V) = 0$$

$$\rho C_p(\boldsymbol{v}\nabla T) + \nabla(-k\nabla T) = Q_{th}$$

$$\rho\left[v_x\frac{\partial v_x}{\partial x} + v_y\frac{\partial v_x}{\partial y}\right] = -\frac{\partial P}{\partial x} + \frac{\partial}{\partial x}\left[\mu\left(2\frac{\partial v_x}{\partial x} - \frac{2}{3}(\nabla\boldsymbol{v})\right)\right] + \frac{\partial}{\partial y}\left[\mu\left(\frac{\partial v_x}{\partial y} + \frac{\partial v_y}{\partial x}\right)\right]$$

$$\rho\left[v_x\frac{\partial v_y}{\partial x} + v_y\frac{\partial v_y}{\partial y}\right] = -\frac{\partial P}{\partial y} + \frac{\partial}{\partial x}\left[\mu\left(\frac{\partial v_y}{\partial x} + \frac{\partial v_x}{\partial y}\right)\right] + \frac{\partial}{\partial y}\left[\mu\left(2\frac{\partial v_y}{\partial y} - \frac{2}{3}\nabla\boldsymbol{v}\right)\right] + \rho g$$

$$\nabla(\rho\boldsymbol{v}) = 0 \qquad (9)$$

The set of partial differential, Equations 9, was solved with the previous boundary conditions (Equations 2, 3, 4, 7) but one more condition on fluid velocity was added at the walls:

$$v_x = v_y = 0 \qquad (10)$$

This two-dimensional model actually includes five variables namely potential, temperature, pressure and velocity vector. Equations 9 are strongly coupled by means of temperature and current density. Such coupling would normally require the simultaneous solution of the five variable equations (9) on a mesh containing, in our case, about 100 000 nodes, leading to a huge memory requirement (up to 128 Mo for the half cell presented in Fig. 1) and a long iterative process.

The results were obtained within four hours using an IBM® RISC 6000/43P workstation equipped with 96 Mo RAM and a 192 Mo swap by use of an alternate algorithm [23] solving, in sequence, each equation of (9). This process was iterated until convergence was obtained simultaneously for potentials, temperatures and velocity.

Some numerical convergence problems were encountered due to an unfavourable advection/conduction ratio related to the non-dimensional mesh Peclet number defined as

$$Pe_M = \frac{\rho C_p v}{k}\Delta l \qquad (11)$$

where v is the magnitude of the velocity vector and Δl is the mesh length in the flow direction. This problem was solved by use of a fine mesh comprising 250 000 nodes in order to maintain the value of Pe_M at less than 2.

Convection has no effect on the potential and current distributions, but Fig. 8 shows that the temperature profiles are slightly modified when the Navier–Stokes equations are taken into account. Surprisingly, it was still necessary to increase the value of the thermal conductivity of the KF–2HF electrolyte up to $20\,W\,m^{-1}\,K^{-1}$ to obtain a convenient temperature distribution in this calculation. The actual velocities are unknown in such a molten salt cell, but the vector velocity field appears appropriate even if a maximum velocity as high as $0.45\,m\,s^{-1}$ may be an overestimation (Fig. 9). This result indicates that free convection due to gravity effects is not so influential as initially thought. Actually the inner convection is probably only governed by the gas bubbles evolving at each electrode. An improved model describing the peculiar effects of evolving fluorine and hydrogen bubbles on the cell hydrodynamics is being studied.

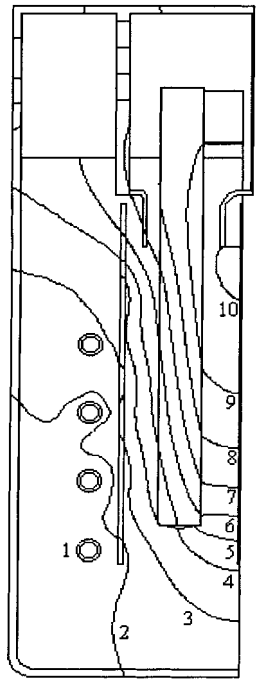

Fig. 7. Temperature profiles computed with $k = 20\,W\,m^{-1}\,K^{-1}$. Temperature: (1) 325 K; (2) 331 K; (3) 337 K; (4) 343 K; (5) 349 K; (6) 355 K; (7) 361 K; (8) 367 K; (9) 373 K; (10) 379 K.

6. Conclusions

Based on the coupled charge and thermal transfer model presented here, the electrical and thermal behaviour of a fluorine cell is now well understood. It is possible to optimize the electrolyser geometry in order to reduce the cell voltage and, thus, the effective cost of industrial cells. At the present time, we are developing a new model to take into account the complex bubble effects encountered in fluorine production to make the model more efficient.

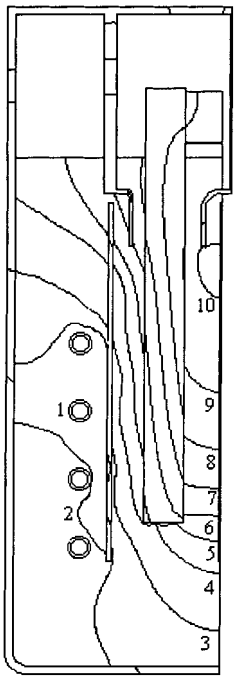

Fig. 8. Temperature profiles with convection. Temperature: (1) 325 K; (2) 332 K; (3) 339 K; (4) 346 K; (5) 353 K; (6) 360 K; (7) 367 K; (8) 374 K; (9) 381 K; (10) 388 K.

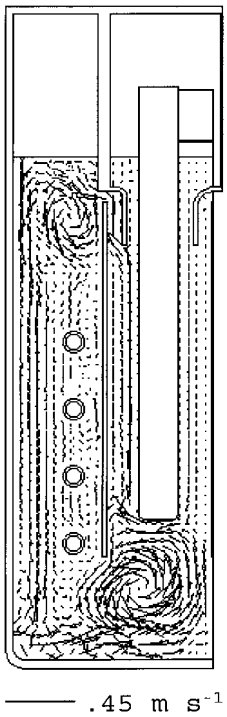

Fig. 9. Velocity vectors (modelled with free convection).

References

[1] T. Z. Fahidy, *J. Appl. Electrochem.* **22** (1992) 125.
[2] J. Divisek and B. Steffen, *Proc. Electrochem. Soc.* **93-14** (Chlor-Alkali and Chlorate Production and New Mathematical and Computational Methods in Electrochemical Engineering) (1993) 297.
[3] T. Z. Fahidy, *Proc. Electrochem. Soc.* ('Fundamentals of Electrochemical Process Design: A Tutorial and Anodic Processes: Fundamental and Applied Aspects') **95–11** (1995) 185.
[4] R. J. Moreau and D. Ziegler, *Metall. Trans. B.* **19B**(5) (1988) 737.
[5] Z. M. Turinskii, *Tsvetn. Met.* (*Moscow*) **11** (1986) 36.
[6] T. Tvedt and H. G. Nebell, *Light Met.* (Warrendale, PA) (1988) 567.
[7] Y. Bertaud, S. Bouvet, A. P. Lamaze, G. Baluais and I. Ronga- Lefebvre, *J. Phys. IV (France)* **4** (1994) 199.
[8] J. P. Caire, H. Roustan, F. Nicolas and P. Pham, *Récents progrès en Génie des Procédés* **49**(10) (1996) 289.
[9] L. Bai and B. E. Conway, *J. Appl. Electrochem.* **18**(6) (1988) 839.
[10] L. Gao, S. Y. Qian and B. E. Conway, *ibid.* **25**(1) (1995) 6.
[11] L. Bai and B. E. Conway, *ibid.* **20**(6) (1990) 925.
[12] J. P. Caire, H. Roustan, F. Nicolas and P. Pham, *Récents progrés en Génie des Procédés* **49**(10) (1996) 307.
[13] M. Jaccaud and F. Nicolas, *Techniques de l'Ingénieur* **J 6020** (1990), 1453.
[14] P. Massé, 'FLUX-EXPERT un système d'aide à la conception de logiciels', PhD INPG-Grenoble, France (1983).
[15] O. C. Zienkiewich, 'The Finite Element Method', McGraw-Hill, New York (1977).
[16] I. Roušar, K. Micka and A. Kimla, 'Electrochemical Engineering II', Chemical Engineering Monographs 21B, Elsevier, Amsterdam (1986), p. 253.
[17] C. Madore, A. C. West, M. Matlosz and D. Landolt, *Electrochim. Acta* **37**(1) (1992) 69.
[18] J. P. Caire, L. Ben Abdallah, P. Ozil and F. Nicolas. 'Electrochemical Engineering and Energy' (edited by F. Lapicque, A. Storck and A. A. Wragg), Plenum, New York (1994), p. 217.
[19] P. Massé, invited paper, Intermag Conference, Hamburg, FRG, 1984, *IEEE Trans. Mag.* **20** (1984) 1885.
[20] H. Roustan, J. P. Caire and F. Nicolas, Journées d'Electrochimie 95, Strasbourg, France, 29 May–1 June 1995, *Proceedings* (1995) CO 9–6.
[21] V. Poulbot, Contribution à l'étude des champs électriques trés basses fréquences en milieu océanique: Electromètre expérimental haute sensibilité; modélisation du système à l'aide d'éléments finis interfaciaux, PhD Ecole Centrale de Lyon, Lyon, France (1993).
[22] F. Nicolas and D. Rabiot, COMURHEX Report (September, 1994).
[23] H. Roustan, Unpublished results.
[24] O. Levenspiel, 'Engineering Flow and Heat Exchange', Plenum, New York (1984), p. 174.
[25] G. Prentice, 'Electrochemical Engineering Principles', Prentice Hall, New York (1991), p. 261.

Appendix

As an example, we describe here the process leading to a specific F.E. equation in order to solve any physical problem ruled by the Laplace equation. The Laplace equation to be solved on a domain Ω reads as

$$\nabla(-\sigma\mathbf{\nabla}V) = 0 \tag{1}$$

For an electrolyser, the boundary conditions imposed at an interface $\partial\Omega$ are

$$V = \text{constant} \tag{2}$$

$$-\sigma\mathbf{\nabla}\mathbf{V}\boldsymbol{n} = 0 \tag{3}$$

$$-\sigma\mathbf{\nabla}\mathbf{V}\boldsymbol{n} = JNF = \text{constant} \tag{4}$$

Using an arbitrary α_i test function, Equation 1 can be transformed in the integral equation

$$\iint_{\Omega} \alpha_i \nabla(-\sigma\mathbf{\nabla}\mathbf{V})\,\mathrm{d}x\,\mathrm{d}y = 0 \tag{5}$$

Since for any scalar p and vector $\boldsymbol{A}$

$$\mathbf{\nabla}(p\boldsymbol{A}) = p\nabla\boldsymbol{A} + \boldsymbol{A}\mathbf{\nabla}p \text{ and } p\nabla\boldsymbol{A} = \nabla(p\boldsymbol{A}) - \boldsymbol{A}\mathbf{\nabla}p \tag{6}$$

Equation 5 may be written as

$$\iint_{\Omega} \alpha_i \nabla(-\sigma \nabla V) = \iint_{\Omega} \nabla(-\alpha_i\ \sigma \nabla V) + \iint_{\Omega} \sigma \nabla V \nabla \alpha_i \tag{7}$$

Since $\iint_{\Omega} \nabla \boldsymbol{A}\, \mathrm{d}x\, \mathrm{d}y = \int_{\partial\Omega} \boldsymbol{A}\, \boldsymbol{n}\, \mathrm{d}l$, then

$$\iint_{\Omega} \nabla(-\alpha_i \sigma \nabla V) = \int_{\partial\Omega} -\alpha_i \sigma \nabla V \cdot \boldsymbol{n}\, \mathrm{d}l \tag{8}$$

The boundary conditions are used to write

$$\int_{\partial\Omega} -\alpha_i\, \sigma \nabla V \boldsymbol{n}\, \mathrm{d}l = \int_{\partial\Omega} \alpha_i\, JNF\, \mathrm{d}l \tag{9}$$

Then Equations 5, 7 and 8 lead to

$$\iint_{\Omega} \sigma\ \nabla \alpha_i \nabla V\, \mathrm{d}x\, \mathrm{d}y = -\int_{\partial\Omega} \alpha_i\, JNF\, \mathrm{d}l \tag{10}$$

In the Galerkin formulation, V is approximated on each finite element using a Lagrange polynomial function α_j and the value of potential V_j at node j

$$V = \sum_j \alpha_j V_j$$

Using this approximation in Equation 10 leads to

$$\left(\iint_{\Omega} \sigma \nabla \alpha_j\ \nabla \alpha_i\, \mathrm{d}x\, \mathrm{d}y \right) V_j = -\int_{\partial\Omega} \alpha_i\, JNF\, \mathrm{d}l \quad \forall i, \forall j \tag{11}$$

Equation 1 is then transformed in a set of equations expressed in matrix form as

$$MI = K_S \tag{12}$$

where matrices $M = \left[MV_{i,j}\right]$, $I = [V_i]$ and $K_S = [KSV_i]$ are all made up of two generic integrals

$$MV_{i,j} = \iint_{\Omega} \sigma \nabla \alpha_j \nabla \alpha_i\, \mathrm{d}x\, \mathrm{d}y \tag{13}$$

$$KSV_i = \int_{\partial\Omega} -\alpha_i\, JNF\, \mathrm{d}l \tag{14}$$

All these integrals are preprogrammed as Fortran subroutines and are found in a F.E. data base. A specific module named 'GENERE' using such predefined integrals allows the user to describe each term of the matrices $\boldsymbol{M}$, $\boldsymbol{I}$ and $\boldsymbol{K}_S$. In the same way, the physical properties of each region, such as the electric conductivity, σ, and the boundary conditions are described by the user as Fortran routines in a specific module named 'PROPHY'.

After Fortran compilation and linking to the general solver code, the user has a new F.E. equation able to solve the Laplace equation for any physical problem defined with the boundary conditions (Equations 2–4).

The whole computing process is then very simple:

(i) The 2D or 3D problem physical geometry is drawn using a specific C.A.O. tool. Each region is described and meshed using triangular or quadrangular finite elements.
(ii) The physical properties are described for each region, and an appropriate resolution algorithm is selected in a module named 'PROPHY'.
(iii) The problem is solved using a module named 'SOLVER'.
(iv) The numerical results are obtained with the help of a graphical tool named 'XPLOIT'.